



Improved cathode/electrolyte interface of SOFC

Nicolas Hildenbrand^{a,*}, Bernard A. Boukamp^a, Pieter Nammensma^b, Dave H.A. Blank^a

^a MESA+ Institute for Nanotechnology, University of Twente, 7500AE Enschede, The Netherlands

^b Energy Center Netherlands, P.O. Box 1, 1755ZG Petten, the Netherlands

ARTICLE INFO

Article history:

Received 1 September 2009

Received in revised form 30 November 2009

Accepted 28 January 2010

Available online 24 February 2010

Keywords:

SOFC

Cathode

Impedance

LSCF

PLD

ABSTRACT

The electrochemical performance of porous $\text{La}_{0.6}\text{Sr}_{0.4}\text{Co}_{0.2}\text{Fe}_{0.8}\text{O}_{3-\delta}$ (LSCF) cathodes is improved by inserting a dense LSCF layer. A 200 nm thin layer is deposited on the electrolyte substrate by pulsed laser deposition, prior to the screen printing process. This procedure enhances the adherence of the porous cathode layer to the electrolyte and allows a lower sintering temperature, which reduces grain growth during sintering. In air a decrease in polarization resistance with a factor of 3 is observed for electrodes sintered at 1100 °C. The apparent electrolyte resistance is also reduced with the dense PLD layer. A remarkable change in P_{O_2} dependence is observed for the Gerischer parameters that describe part of the electrode impedance, indicating a possible change in the oxygen transfer mechanism.

© 2010 Elsevier B.V. All rights reserved.

1. Introduction

The optimization of the SOFC performance at intermediate temperatures (600–800 °C) depends strongly on efficient cathode materials and structures. The $\text{La}_{0.6}\text{Sr}_{0.4}\text{Co}_{0.2}\text{Fe}_{0.8}\text{O}_{3-\delta}$ perovskite material (LSCF) is an interesting candidate. Its reactivity with the standard zirconia electrolyte can be suppressed by using an yttria-stabilized ceria interlayer. The polarization resistance of the cathode is also dependent on the microstructure and thus on the preparation process [1,2]. In a separate report the influence of the sintering temperature on microstructure and polarization resistance of screen printed LSCF cathodes is presented [3]. A very strong sintering temperature dependence was noted, cathodes sintered at 1100 °C showed poor adherence, while cathodes sintered at 1300 °C suffered from excessive grain growth, leading to a low porosity structure and hence a high polarization resistance. The optimum in cathode properties was found for a sintering temperature of 1200 °C. Lowering the sintering temperature has the advantage of smaller grain sizes, which will increase the active surface area for the oxygen exchange and reduction reaction. To improve the adherence of the porous electrode to the electrolyte it is proposed to apply a thin, dense LSCF layer to the electrolyte before the screen printing process. Pulsed laser deposition (PLD or laser ablation) has the advantage of stoichiometric transfer and a strong bonding with the substrate of the deposited composition. In this report the performance of a PLD-enhanced cathode structure is studied with electrochemical impedance spectroscopy (EIS) as function of

temperature and oxygen partial pressure. The results are compared with the performance of the regular screen printed cathode.

2. Experimental

Symmetrical two-electrode cells were prepared by tape-casting and screen printing processes. Tape-casted yttria-partially stabilized zirconia (3YSZ, Tosoh) was used as electrolyte. Yttria-doped ceria (YDC, Praxair) was provided as interlayer by screen printing and sintered at 1400 °C on both sides of the tape-casted 3YSZ electrolyte. Two identical porous electrodes of $\text{La}_{0.6}\text{Sr}_{0.4}\text{Co}_{0.2}\text{Fe}_{0.8}\text{O}_{3-\delta}$ (LSCF, Praxair) were then screen printed on both sides of the electrolyte and sintered at 1100 °C to complete the reference samples (further denoted by P). For the PLD-enhanced samples (denoted by DP) dense thin layers of LSCF were deposited by pulsed laser deposition on the YDC interlayer, prior to the screen-printing of the porous LSCF electrodes. The pulsed laser deposition was performed with a KrF excimer laser, using a fluency of 2.6 J/cm² and a frequency of 20 Hz. The LSCF target was provided by placing an isostatically pressed LSCF pellet on a rotating holder. The laser ablation occurred in a vacuum chamber in 0.02 mbar oxygen ambient. The YDC/3YSZ/YDC substrates were heated to 750 °C during deposition. Schematic representation of the two different samples (P and DP) is presented in Fig. 1.

The measurement of the electrochemical properties of the different cells were performed at open-circuit voltage in synthetic air as a function of temperature between 800° and 300 °C at 50 °C intervals, and as a function of oxygen partial pressure at 600 °C. The impedance characteristics were measured with a Solartron 1250 FRA combined with a 1287 electrochemical interface over a frequency range of 65,535 Hz to 10 mHz in a pseudo 4-electrode set up (separate current and voltage probe leads).

* Corresponding author. University of Twente, P.O. Box 217, 7500AE Enschede, the Netherlands. Tel.: +31 534892556; fax: +31 534893595.

E-mail address: n.hildenbrand@utwente.nl (N. Hildenbrand).

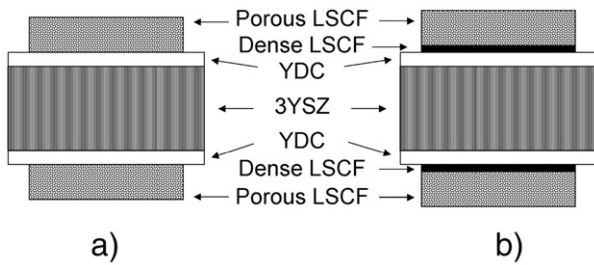


Fig. 1. Scheme of (a) sample P and (b) sample DP.

The impedance data were validated with a Kramers–Kronig transform program [4] and analysed with the software package ‘Equivalent Circuit’ [5].

3. Result and discussion

3.1. Microstructure

The cross section of a typical symmetrical cell is shown in the SEM micrograph in Fig. 2a. The electrolyte thickness is 92 μm , the electrodes on both sides of the cell are 53 μm thick, the electrode

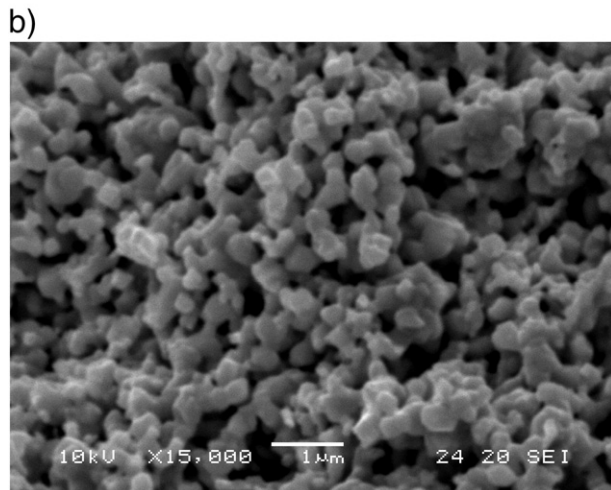
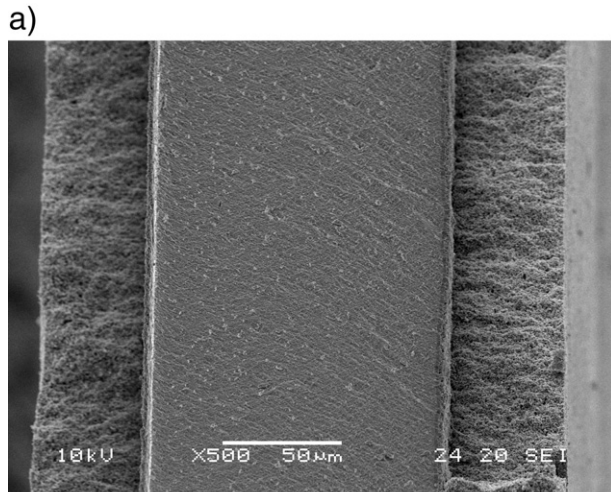


Fig. 2. (a) SEM micrograph of a cross section of the symmetrical cell. (b) SEM micrograph of the microstructure of the LSCF porous cathode.

and the electrolyte are separated by a YDC interlayer approximately 3 μm thick. Mean grain size of the porous LSCF cathode sintered at 1100 $^{\circ}\text{C}$ is 0.50 μm . In the DP sample the dense PLD-LSCF layer is 200 nm thick, completely covering the rough YDC surface. Fig. 3 shows that there is a very good adhesion to the YDC interlayer.

3.2. Temperature dependence

Fig. 4a shows the impedance characteristics of the samples D and DP at 400 $^{\circ}\text{C}$ in air. The high frequency semicircle that becomes visible at low temperatures is attributed to the grain boundary dispersion of the electrolyte. The low frequency dispersion represents the electrode response. Fig. 4b shows the impedance characteristics at 600 $^{\circ}\text{C}$ in air. In this range of temperature, only the electrode response can be observed. At high temperatures (800 $^{\circ}\text{C}$, Fig. 4c) a low frequency semi-circle develops which can be attributed to gas phase limitation in the porous electrode. The introduction of the PLD-LSCF layer results in a decrease of the apparent electrolyte resistance by a factor of 1.25 and of the polarization resistance by a factor of 3, see Fig. 4d. A comparison of typical values for both samples is presented in Table 1. The temperature dependence of the electrolyte resistance and the polarization resistance is presented in Fig. 4d. The observed activation energies for the electrolyte conductivity are 0.74 eV (DP) and 0.73 eV (P). As the YDC/3YSZ/YDC electrolytes are similar for type P and DP samples, the decrease of the electrolyte resistance by a factor of 1.25 for DP samples can only be explained by an improvement in the contact between the electrode and the electrolyte. Gazzarri et al. [6] observed a shift to the right of the electrode dispersion in the impedance graph when comparing a normal electrode and an electrode with delaminated cathode area. This phenomenon was explained by a reduction in the ion conduction area, caused by delamination thus apparently increasing the electrolyte resistance. In the case of type P and DP samples, a porous electrode with a porosity estimated to 20% covers at most 80% of the surface. Hence by introducing a dense layer, the contact between the electrode and the electrolyte becomes 100% which is a factor 1.25 higher than 80%.

For the polarization resistances 1.29 eV (DP) and 1.34 eV (P) are found, which values are consistent with literature data [7–10]. All spectra for both types of samples could be modeled with the equivalent circuit presented in Fig. 5a. The high frequency grain boundary contribution is only observable at low temperatures, while the low frequency gas phase limitation dispersion is only visible at high temperatures ($\sim 800^{\circ}\text{C}$). The main feature is the well-

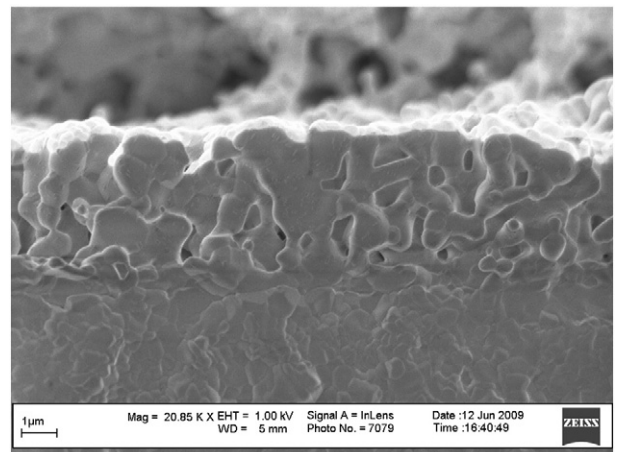


Fig. 3. SEM micrograph of a cross section of a symmetrical cell with a LSCF layer deposited by pulsed laser deposition.

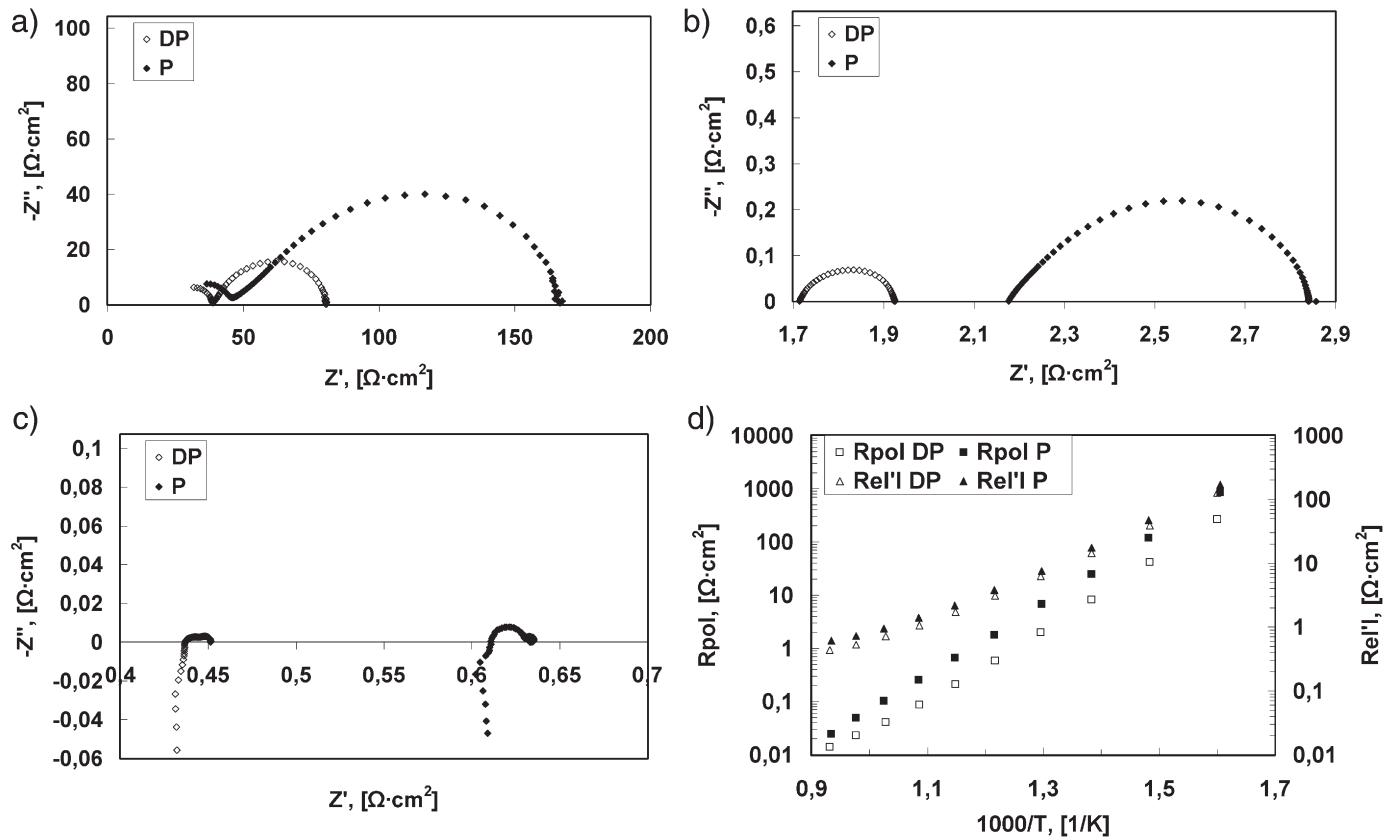


Fig. 4. (a) Impedance characteristics of sample D and DP in air at (a) 400 °C, (b) 600 °C and (c) 800 °C. (d) Electrolyte and polarization resistance as a function of temperature in air.

documented Gerischer dispersion (or chemical impedance [11–13]), here expressed as:

$$Z_G(\omega) = Z_0 / \sqrt{K_a + j\omega}. \quad (1)$$

Besides this Gerischer element, which is typical for the LSCF-type cathodes, an overlapping semicircle contribution (R_{lf} Q_{lf}) was systematically observed. This dispersion, which has not been reported previously, is tentatively assigned to the redox process in the LSCF-cathode. The overall CNLS-modeling error was generally less than 1%, as can be seen from the typical residuals graph in Fig. 5b. For the DP and P type samples, Z_0 and R_{lf} were following an Arrhenius behaviour with activation energies equal to 0.80 eV and 1.31 eV, respectively. For the temperature dependence in air, the comparison of the circuit parameters for the DP and P type samples did not reveal significant differences that would directly explain the improved performance of the DP-cathodes. However, as will be shown in the next paragraph, the oxygen partial pressure dependence shows remarkable differences between the DP and P type samples.

3.3. Oxygen partial pressure dependence.

The P_{O_2} dependence of both types of cathodes was measured at 600 °C. The electrolyte resistance in both cases was, as expected, independent of

P_{O_2} oxygen partial pressure. The polarization resistance decreases with increasing oxygen partial pressure obeying:

$$R_p = R_0 \cdot P_{O_2}^{-n} \quad (2)$$

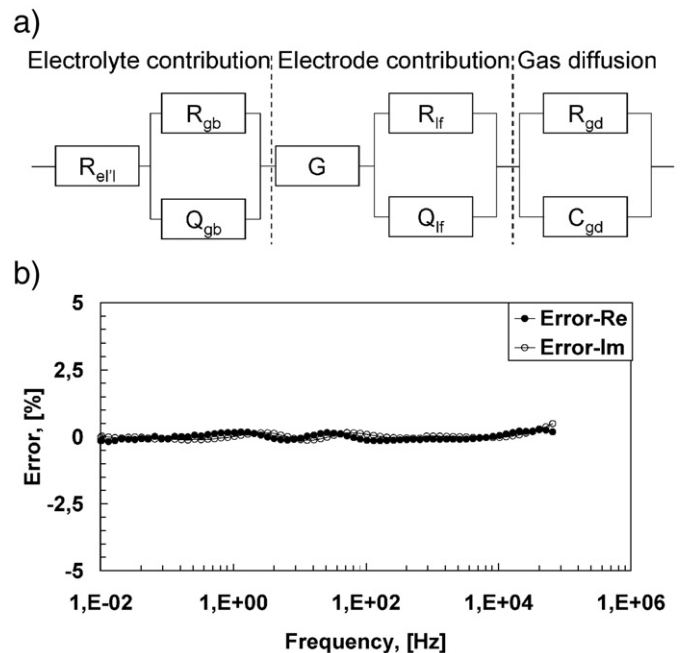


Fig. 5. (a) Equivalent circuit used to fit the impedance spectra. (b) Error between measurement and model as function of frequency for DP sample at 500 °C in air.

Table 1
Comparison of polarization resistances for samples DP and P in air.

| Temperature | 800 °C | 600 °C | 500 °C | |
|-------------|--------|--------|--------|----------------------|
| DP | 0.015 | 0.21 | 2.0 | [Ω cm ²] |
| P | 0.025 | 0.67 | 6.8 | [Ω cm ²] |

with $n=0.20$ for the P-sample and $n=0.17$ for the DP-sample. According to Takeda et al., a $P_{O_2}^{-0.25}$ dependence can be attributed to adsorption and surface exchange limitation [14]. Again, the polarization resistance was reduced by a factor between 3 and 4 when comparing sample DP to sample P (Fig. 6). Following the ALS model [11] the Gerischer parameters Z_0 and K_a from Eq. (1) are related to material and microstructure parameters by:

$$Z_0 = \frac{RT}{2F^2 c_v(1-\varepsilon)} \sqrt{\frac{\tau}{D_v}}, \text{ and } K_a = \frac{A a r_0 (\alpha_f + \alpha_b)}{c_v(1-\varepsilon)} \quad (3)$$

with c_v the vacancy concentration, ε the cathode porosity, τ the tortuosity. D_v is the vacancy diffusion coefficient, A the thermodynamic factor ($=\partial \ln(P_{O_2}) / 2\partial \ln(c_v)$), a is the specific surface area, r_0 is the exchange neutral flux density and α_f and α_b are constants of the order of unity that depend on the specific mechanism of the exchange reaction [11].

For the regular porous cathode, P, the P_{O_2} dependence of Z_0 and K_a were $P_{O_2}^{0.17}$ and $P_{O_2}^{0.62}$ respectively. This is in reasonable agreement with the results obtained by Adler et al.: a $P_{O_2}^{0.30}$ dependence for Z_0 and a $P_{O_2}^{0.64}$ dependence for K_a . However, the DP-cathodes showed a much higher P_{O_2} dependence for Z_0 , with $Z_0 \propto P_{O_2}^{0.76}$, while for K_a the opposite was found: $K_a \propto P_{O_2}^{0.25}$, less than half the value for the regular cathode. The addition of a thin dense layer thus seems to change the oxygen reduction/incorporation mechanism significantly. On the one hand, K_a increases by a factor 2 at low P_{O_2} and a factor of 4 at high P_{O_2} for the enhanced DP-cathode, indicating a more effective surface exchange. On the other hand, Z_0 decreases by a factor of 3 at low P_{O_2} and a factor of 30 at high P_{O_2} for the DP-cathode. As the cathode composition is the same for the DP- and P-cathode assemblies, the improvement of the surface exchange can be due to an improved 'footprint' of the cathode

on the electrolyte. This allows the transfer of oxygen ions from the cathode bulk to the electrolyte over the entire interface, while surface diffusion and transfer in the triple phase boundary zone is suppressed. Besides the Gerischer parameters, the overlapping semicircle contribution ($R_{if} Q_{if}$) was also studied. Whereas Q_{if} was nearly P_{O_2} independent, the values for R_{if} were virtually identical for P and DP type samples and had a reaction order of -0.30 . The ($R_{if} Q_{if}$) contribution could thus be attributed to a bulk process in the cathode rather than to the electrolyte/cathode interface.

4. Conclusion

The cathode/electrolyte interface is playing an important role in the overall performance of the cathode. Introduction of a thin, dense $\text{La}_{0.6}\text{Sr}_{0.4}\text{Co}_{0.2}\text{Fe}_{0.8}\text{O}_{3-\delta}$ layer is introduced by Pulsed Laser Deposition at the electrolyte/cathode interface improves the adherence of the cathode to the electrolyte and allows a lower sintering temperature during the process. A thin, dense LSCF layer results in a decrease of the polarization resistance of the cathode by a factor 3. The oxygen partial pressure dependence shows that the mechanism of oxygen reduction changes possibly indicating an improvement in the surface exchange step. Further analysis with a Finite Element Method modeling software will be carried out to fully understand this improvement and mechanisms change.

Acknowledgement

The authors gratefully acknowledge financial support from SenterNovem, an agency of the Dutch Ministry of Economic Affairs promoting sustainable development and innovation.

References

- [1] H.T. Lim, et al., *J. Power Sources* 180 (2008) 92.
- [2] M. Backhaus-Ricoult, *Solid State Sciences* 10 (2008) 670.
- [3] N. Hildenbrand, B.A. Boukamp, D.H.A. Blank, in preparation.
- [4] B.A. Boukamp, *J. Electrochem. Soc.* 142 (6) (1995) 1885.
- [5] B.A. Boukamp, *Solid State Ionics* 20 (1986) 31.
- [6] J.I. Gazzarri, O. Kesler, *J. Power Sources* 167 (2007) 430.
- [7] J.D. Sirman, J.A. Lane, J.A. Kilner, *Ionic and Mixed Conducting Ceramics III*, in: T.A. Ramanarayanan, W.L. Worrell, H.L. Tuller, A.C. Khandkar, M. Mogensen, W. Gopel (Eds.), *The Electrochemical Society Proceedings Series*, 97–24, Pennington, NJ, 1997, p. 57.
- [8] S.P. Jiang, *Solid State Ionics* 146 (2002) 1.
- [9] J.-M. Bae, B.C.H. Steele, *Solid State Ionics* 106 (1998) 247.
- [10] A. Esquirol, N.P. Brandon, J.A. Kilner, M. Mogensen, *J. Electrochem. Soc.* 151 (2004) A1847.
- [11] S.B. Adler, J.A. Lane, B.C.H. Steele, *J. Electrochem. Soc.* 143 (1996) 3554.
- [12] Y. Lu, C. Kreller, S.B. Adler, *J. Electrochem. Soc.* 156 (2009) B513.
- [13] B.A. Boukamp, H.J.M. Bouwmeester, *Solid State Ionics* 157 (2003) 29.
- [14] Y. Takeda, R. Kanno, M. Noda, Y. Tomida, O. Yamamoto, *J. Electrochem. Soc.* 134 (1987) 2656.

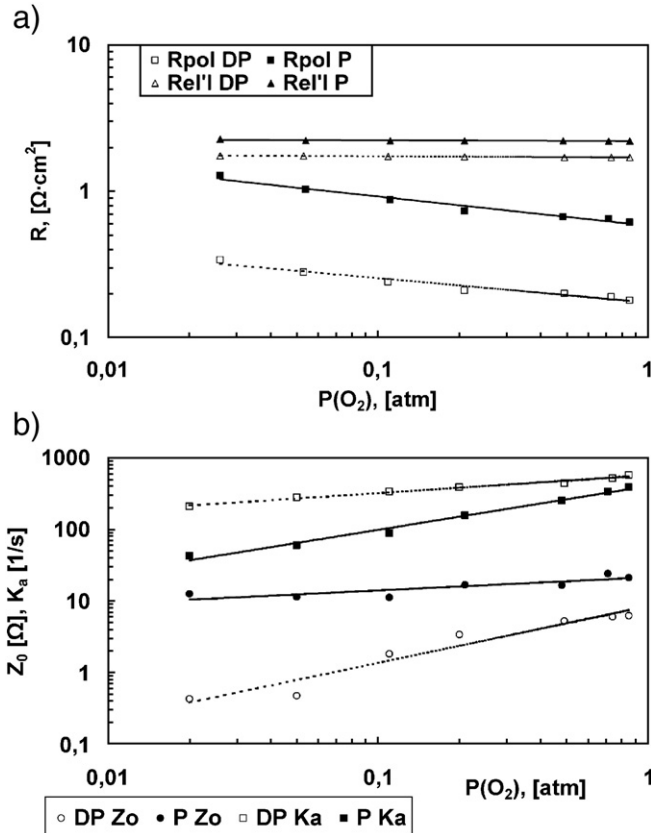


Fig. 6. (a) Electrolyte and polarization resistance as a function of oxygen partial pressure at 600 °C. (b) Evolution of Gerischer-parameters of the equivalent circuit as function of the oxygen partial pressure at 600 °C.